UNIVERSITY OF AMSTERDAM

UvA-DARE (Digital Academic Repository)

Detection of small atom numbers through image processing

Ockeloen, C.F.; Tauschinsky, A.F.; Spreeuw, R.J.C.; Whitlock, S.

DOI
10.1103/PhysRevA.82.061606
Publication date
2010
Document Version
Final published version
Published in
Physical Review A

Link to publication

Citation for published version (APA):
Ockeloen, C. F., Tauschinsky, A. F., Spreeuw, R. J. C., & Whitlock, S. (2010). Detection of small atom numbers through image processing. *Physical Review A*, *82*(6), 061606(R). https://doi.org/10.1103/PhysRevA.82.061606

General rights
It is not permitted to download or to forward/distribute the text or part of it without the consent of the author(s) and/or copyright holder(s), other than for strictly personal, individual use, unless the work is under an open content license (like Creative Commons).

Disclaimer/Complaints regulations
If you believe that digital publication of certain material infringes any of your rights or (privacy) interests, please let the Library know, stating your reasons. In case of a legitimate complaint, the Library will make the material inaccessible and/or remove it from the website. Please Ask the Library: https://uba.uva.nl/en/contact, or a letter to: Library of the University of Amsterdam, Secretariat, P.O. Box 19185, 1000 GD Amsterdam, The Netherlands. You will be contacted as soon as possible.

UvA-DARE is a service provided by the library of the University of Amsterdam (https://dare.uva.nl)

Download date:13 Oct 2026

PHYSICAL REVIEW A **82**, 061606(R) (2010)

Detection of small atom numbers through image processing

C. F. Ockeloen, A. F. Tauschinsky, R. J. C. Spreeuw,* and S. Whitlock
Van der Waals–Zeeman Institute, University of Amsterdam, Valckenierstraat 65, 1018 XE Amsterdam, The Netherlands
(Received 13 July 2010; published 16 December 2010)

We demonstrate improved detection of small trapped atomic ensembles through advanced postprocessing and optimal analysis of absorption images. A fringe-removal algorithm reduces imaging noise to the fundamental photon-shot-noise level and proves beneficial even in the absence of fringes. A maximum-likelihood estimator is then derived for optimal atom-number estimation in well-localized ensembles and is applied to real experimental data to measure the population differences and intrinsic atom shot noise between spatially separated ensembles each comprising between 10 and 2000 atoms. The combined techniques improve our signal-to-noise ratio by a factor of 3, to a minimum resolvable population difference of 17 atoms, close to our ultimate detection limit.

DOI: 10.1103/PhysRevA.82.061606 PACS number(s): 67.85.−d, 37.25.+k, 07.05.Pj

Trapped ultracold atoms and quantum degenerate gases are novel systems for the study of many-body quantum physics [1] and are key to new technologies such as trapped-atom interferometers [2] and atomic clocks [3]. This is exemplified by recent experiments on number or spin squeezing and entanglement between small atomic ensembles [4], which could serve as a resource for quantum metrology and quantum information science. Essential to such applications is the ability to precisely measure the populations of a pair of atomic ensembles in, for example, a double-well potential for Josephson physics or atom interferometry [2,5–7], or the spin states of an atomic clock. Upon readout the interferometric phase can be mapped to a population difference and the two ensembles are imaged to different regions of a charge-coupled device (CCD) camera. The relative population is robust against common-mode technical fluctuations such as probe noise or trap loading efficiency. However, imaging noise and intrinsic atom-number fluctuations (atom shot noise) typically limit measurement precision.

Here we demonstrate improved detection of trapped ensembles of ultracold atoms through advanced postprocessing and optimal analysis of laser-illuminated absorption images. This allows us to better measure the intrinsic atom-number fluctuations in a magnetic lattice potential. We focus on small ensembles localized close to the limit of our optical resolution in the presence of added imaging noise. First we apply a fringe-removal algorithm to reduce imaging noise to the fundamental photon-shot-noise level. We then establish the ultimate limit for measuring the relative populations based on the Cramér-Rao bound (CRB) and derive maximum-likelihood estimators that attain this limit [8]. These optimal analysis techniques provide the basis to improve the readout of trapped-atom interferometers to the quantum limit or to better resolve number squeezing and entanglement.

In our experiment we prepare up to a total of $N = 4 \times 10^3$ ^{87}Rb atoms in a multiwell trap formed by a current through a Z-shaped wire and the permanent field of a magnetic-lattice atom chip [9]. Recently we used this setup to study sub-Poissonian atom-number fluctuations in an array of tightly confining microtraps [10]. In this work we position the trap at the edge of the magnetic lattice, 45 μm below the chip surface, to create four potential wells (two deep central wells and two shallow outer wells), each separated by 70 μm. The atoms are evaporatively cooled in this trap to a temperature of $\sim$1 μK, thereby creating independent atomic ensembles, each occupying an area of $\sim 10 \times 50$ μm^2 in our images (Fig. 1). The mean number of atoms is varied by holding the atoms in the trap for 0–4 s at a fixed temperature and partially by reducing the amount of Rb dispensed during loading. For 100 atoms/well the peak atomic density corresponds to $\approx$4 atoms/pixel, close to our typical noise levels limited by optical fringes and photon shot noise.

We perform absorption imaging by briefly exposing the atoms to a nearly homogeneous probe laser, typically tuned to resonance with an atomic transition. The resulting absorption signal A is imaged onto a CCD camera. Subsequently the atoms are ejected from the trap and a reference image R is recorded to normalize intensity variations of the probe. A dark image may also be recorded without the probe to subtract any stray light or CCD dark counts. The two-dimensional atomic density is calculated as $n_x = -\alpha[\ln(A_x/R_x) + s_x(A_x/R_x - 1)]/\sigma_0$ (where x indexes pixels in the images, throughout) [11]. Here $\sigma_0 = 3\lambda^2/2\pi$ is the absorption cross section, α is a dimensionless parameter which depends, for example, on the probe polarization, and $s = I_R/\alpha I_s^0$ is the (spatially dependent) saturation parameter, with I_R the probe intensity at the position of the atoms and $I_s^0 = 1.67$ mW/cm^2 the saturation intensity for our transition.

The experiments employ a back-illuminated deep-depletion CCD camera with a quantum efficiency of about 0.9 at $\lambda =$ 780 nm, a measured gain of $g = 0.87 \pm 0.05$ counts/photon, and a readout noise level of $\sigma_{\mathrm{rd}} \approx 13$ counts. The resolution of our optical system is 9.6 μm (Rayleigh criterion) with a pixel area of $\Delta = (3.3 \pm 0.1\ \mu\mathrm{m})^2$ in the object plane. The probe is slightly inclined with respect to the gold-coated chip surface to create two mirror images of the atoms (Fig. 1) [12]. Correlation of these images provides additional means to distinguish atom shot noise and imaging noise.

We have experimentally optimized our imaging parameters to provide the highest signal-to-noise ratios (SNR) for in-trap imaging. Long exposure times τ tend to lower the effect of photon shot noise; however, blurring or heating due to photon recoil during the imaging pulse tends to increase the effective area a over which the atoms are distributed. Therefore, one finds an optimum intensity and exposure time.

*R.J.C.Spreeuw@uva.nl

 ©2010 The American Physical Society

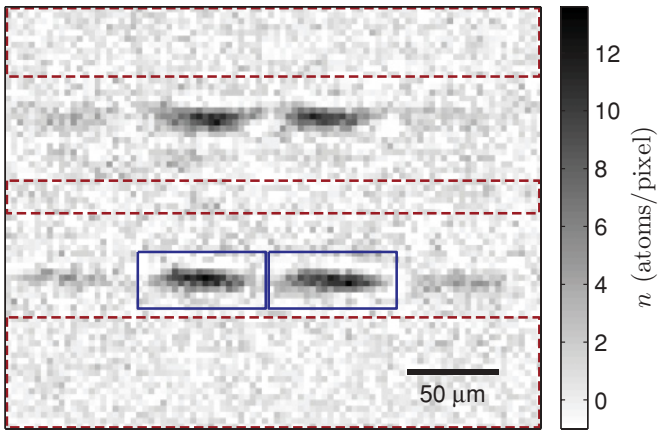

FIG. 1. (Color online) Typical absorption image of the atomic distribution (90 × 71 pixels) for a hold time of 1.6 s. Four independent atomic ensembles are visible (horizontally distributed) with two mirror images (vertically separated). The two centermost clouds each contain ≈400 atoms (≈100 in outermost wells). Dashed boxes indicate the background pixels for the fringe-removal algorithm, and the signal regions are indicated by solid lines.

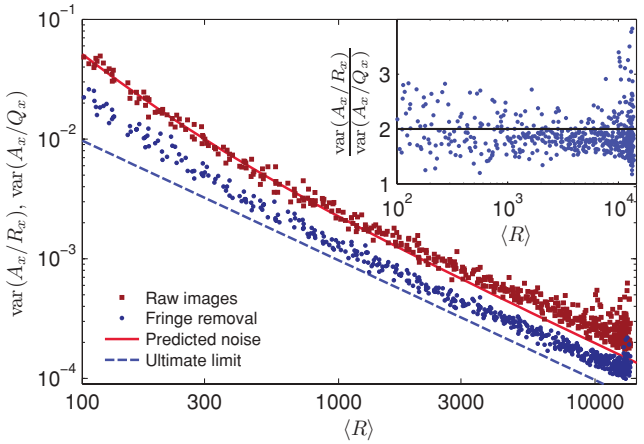

FIG. 2. (Color online) Imaging noise for various probe intensities with and without fringe removal, $\mathrm{var}(A_x/Q_x)$ (circles) and $\mathrm{var}(A_x/R_x)$ (squares), respectively. The predicted photon shot noise plus camera readout noise is shown as a solid line. The dashed line shows the ultimate photon-shot-noise limit.

We measure the SNR in a series of absorption images for constant atom number as a function of both τ and s and find a maximum for $\tau = 50\ \mu$s and $s \approx 0.54$. Finally, we calibrate α by comparing the integrated absorption signal with a second set of images taken after free expansion using a weak probe ($s \approx 0.02$), yielding $\alpha = 3.0 \pm 0.2$. Detection linearity with respect to atom-number variations is confirmed by measuring a fixed ratio between the populations of the center and outer wells. Our typical atom numbers correspond to weak absorption signals ($A_x/R_x \gtrsim 0.8$) for which it can be difficult to extract a signal buried in noise.

In practice additional imaging noise originates from fringes, due to diffraction and interference of the probe beam by optical elements and the atom chip surface. Small vibrations between the absorption and reference images result in imperfect normalization due to fluctuating fringe patterns. This noise can be greatly reduced through the application of a fringe-removal algorithm, while making no assumptions about the atomic distribution. The algorithm works by composing for each absorption image a matching optimal reference image Q constructed as a linear combination of many reference images R_k within a set, $Q_x = \sum_k c_k R_{x,k}$ [13,14]. The method is closely related to that applied to facial recognition [15] and recently in astronomical image analysis for detecting extrasolar planets [16].

To obtain the coefficients c_k we minimize the least squares difference between the absorption and reference images $\sum_x m_x (A_x - Q_x)^2$, within a specified background region ($m_x = 1$) excluding the signal region ($m_x = 0$). Setting partial derivatives with respect to c_j to zero, we obtain a linear system of equations $\sum_k c_k B_{j,k} = \sum_x m_x R_{x,j} A_x$ with the square matrix $B_{j,k} = \sum_x m_x R_{x,j} R_{x,k}$, which can be readily solved for c_k. As a typical data set consists of hundreds of absorption images, we decompose B once using lower-upper (LU) or singular value decomposition and then substitute to obtain c_k for each absorption image [17]. The algorithm is also sufficiently fast to decompose B and process new images in less than 1 s for live processing between experimental cycles.

Figure 2 shows the imaging noise with and without fringe removal, $\mathrm{var}(A_x/Q_x)$ and $\mathrm{var}(A_x/R_x)$, respectively, calculated for a signal-free region (separate from the fringe-removal background region) for various probe intensities. Without fringe removal the measured noise is in good agreement with the expected photon shot noise and readout noise, given our CCD parameters. Application of the fringe-removal algorithm with a basis of ∼250 reference images reduces the measured variances by a factor of 1.9 ± 0.3 over the full range of intensities. Remarkably, even in the absence of fringes, the algorithm reduces the photon-shot-noise contribution originating from R. This is possible since the optimal reference image is the (weighted) average over many reference images, allowing an additional decrease of uncorrelated noise by up to a factor of 2. For our chosen imaging parameters the remaining noise from pixel to pixel has a standard deviation of $\sigma_n = 1.3 \pm 0.3$ atoms, close to the ultimate limit of 1.1 atoms due to photon shot noise in A. There is also a small residual correlated noise component which fluctuates on a length scale comparable to our cloud size with an rms amplitude of 0.06 ± 0.01 atoms.

We wish to measure the total and difference populations $N^{\pm} = N_p \pm N_q$ and the relative population difference N^-/N^+. To establish the limit for extracting these populations from our images we derive the Cramér-Rao bound. The CRB gives a lower bound for the variance of any parameter estimate, independent of the exact procedure used to extract the information [8]. We focus on small atom numbers localized close to the limit of our optical resolution, where the added imaging noise (N independent) dominates over local density fluctuations (spatially resolved shot noise). For our parameters we expect our analysis to be beneficial for $N^+ \lesssim 3000$. We describe our image data as the absorption signal from a pair of atomic ensembles corrupted by uncorrelated additive Gaussian noise $d_{i,x}$ with variance σ_n^2: $n_{i,x} = N_{i,p} p_x + N_{i,q} q_x + d_{i,x}$, where i labels a particular realization. The mean profile of the clouds in the image is represented by the normalized spatial

mode functions p_x and q_x ($\sum_x p_x = \sum_x q_x = 1$). These are determined by the cloud shape and optical resolution of our imaging system and are independent of total atom number. The log-likelihood function is

$$l(N_{p,q}; n_{i,x}) = -\sum_x \frac{(n_{i,x} - N_{i,p}p_x - N_{i,q}q_x)^2}{2\sigma_n^2} + \text{const.} \quad (1)$$

The CRB is then the inverse of the Fisher information matrix, calculated from the second derivatives of l with respect to $N^{\pm}$. We obtain for the CRB

$$\text{cov}(N^+, N^-) \geqslant C = \frac{4\sigma_n^2}{(u^+u^-) - v^2} \begin{pmatrix} u^- & -v \\ -v & u^+ \end{pmatrix}, \quad (2)$$

with the parameters $u^{\pm} = \sum_x (p_x \pm q_x)^2$ and $v = \sum_x (p_x^2 - q_x^2)$. Here $\text{var}(N^+) \geqslant C_{11}$, $\text{var}(N^-) \geqslant C_{22}$, and for the relative atom number,

$$\text{var}\left(\frac{N^-}{N^+}\right) \geqslant \frac{\langle N^-\rangle^2 C_{11} + \langle N^+\rangle^2 C_{22} - 2\langle N^-\rangle\langle N^+\rangle C_{12}}{\langle N^+\rangle^4}. \quad (3)$$

Taking typical numbers from our experiment ($v \approx 0$ and $1/u^{\pm} \approx 30$) we find the single-shot CRB to be $C_{11} = C_{22} = 200$ atoms^2, or a minimum resolvable population difference of 14 atoms. The CRB is also easily applied to estimating the number of atoms within a single ensemble, for which our detection limit is 10 atoms/shot.

The CRB can be attained by a maximum-likelihood estimator (MLE), found by maximizing the log-likelihood function and solving for $N^{\pm}$,

$$\hat{N}_i^{\pm} = \frac{2u^{\mp}}{(u^+u^-) - v^2} \sum_x n_{i,x} \left((p_x \pm q_x) - \frac{v(p_x \mp q_x)}{u^{\mp}} \right). \quad (4)$$

Equation (4) can be interpreted as a sum over the imaged density distribution weighted by $p_x \pm q_x$, where the second term accounts for overlapping and uneven mode functions. This gives a direct measure of the populations while minimizing the influence of noise. The mode functions p_x and q_x can be obtained from the data in a model-independent way by averaging over many images to suppress noise. If p_x and q_x are not spatially separated one can record a set of images where each ensemble is individually populated or apply independent component analysis to isolate signal components [18].

We compare the expected performance of the MLE to naive estimates for $N^{\pm}$ obtained by separately integrating over rectangular subimages containing the left and right ensembles. For this case, the expected variance is $\text{var}(N^{\pm}) \geqslant a\sigma_n^2$, with a the total number of pixels in the integration regions. For regions chosen to include more than 95% of the atomic signal ($a/2 = 10 \times 22$ pixels, Fig. 1) we expect a detection-noise contribution to $\text{var}(N^{\pm})$ of 730 atoms^2, a factor 3.7 larger than the CRB.

We have performed measurements of the relative atom number N^-/N^+ for varying total atom number to resolve intrinsic atom-number fluctuations and demonstrate the improvements gained using maximum-likelihood estimation. Our data set spans 40 hold times between 0 and 4 s, corresponding to varying $\langle N^+\rangle$ from 4×10^3 down to $\sim$20 atoms. For each hold time we repeat the experiment 40 times. Subpixel image registration is applied to align each image to the average to eliminate small fluctuations in the atom cloud positions. The mode functions of the left and right clouds, p_x and q_x respectively, are estimated by averaging all the data and segmenting the result. We then extract from the images the atom-number populations using Eq. (4) and compute the variance $\text{var}(N^-/N^+)$. The expected atom-shot-noise contribution to the variance, accounting for a mean population imbalance, is $1/\langle N^+\rangle - \langle N^-\rangle^2/\langle N^+\rangle^3$.

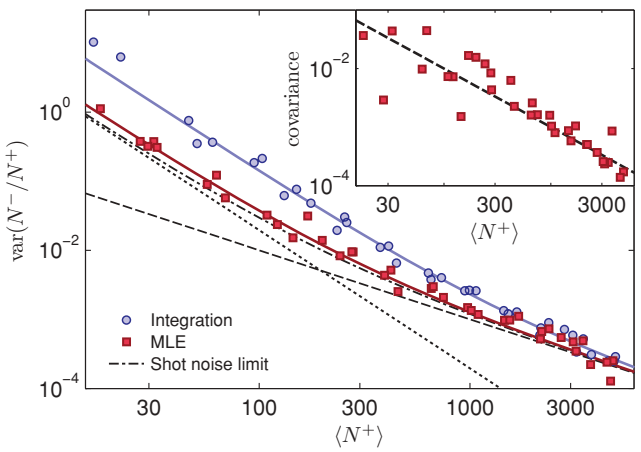

FIG. 3. (Color online) Relative variance as a function of total atom number measured by maximum-likelihood estimation (squares) or straight integration (circles). The dash-dotted line shows the expected fluctuations combining atom shot noise (dashed line) and the minimum detection-noise contribution given by the CRB (dotted line). Solid lines indicate fits for the detection-noise contributions. The inset shows the covariance between N^-/N^+ in the upper and lower mirror images (squares) along with the predicted atom shot noise (dashed line).

Figure 3 shows the measured variance of the relative population for both the MLE and simple integration as a function of $\langle N^+\rangle$. We restrict our analysis to the lower mirror image specified in Fig. 1. For large $\langle N^+\rangle$ both estimation methods yield results which are atom-shot-noise limited. For the integration method the measured variance is limited by detection noise for $\langle N^+\rangle$ below $\sim$1000 atoms. Detection is significantly improved using the MLE, enabling atom-shot-noise-limited detection down to fewer than 300 atoms. To the data we fit the model $\text{var}(N^-/N^+) = \tilde{C}_{22}/\langle N^+\rangle^2 + 1/\langle N^+\rangle$ (for our data $\langle N^-\rangle \approx 0$), to measure the detection-noise contribution. For straight integration we find $\tilde{C}_{22} = (1.3 \pm 0.2) \times 10^3$ atoms^2, whereas for the MLE $\tilde{C}_{22} = 270 \pm 40$ atoms^2, corresponding to a minimum resolvable difference of 17 atoms/shot. The measured noise is slightly larger than the minimum value given by the CRB, but is consistent with the added effect of the residual correlated noise.

We can further distinguish atom-number fluctuations from detection noise in our data by comparing the measured population differences in the two mirror images. Here we expect the detection noise to be uncorrelated, and true atom-number fluctuations to be correlated between the two images. To verify this, we measure N^+ and N^- for both mirror images

separately and calculate the covariance of N^-/N^+ between the upper and lower images for each hold time. The result is shown in the inset of Fig. 3, along with the expected atom shot noise $1/\langle N^+\rangle$. Our data are consistent with atom shot noise over the full range of atom numbers, demonstrating a robust method to observe intrinsic atom-number fluctuations.

To summarize, we have demonstrated improved detection of small atomic ensembles, to close to the ultimate photon-shot-noise limit. A fringe-removal algorithm and maximum-likelihood estimation are applied to absorption images to reach a measured detection sensitivity of 17 atoms/shot for population differences. The measured variance of the relative populations is in excellent agreement with the lower limit given by atom shot noise and the Cramér-Rao bound for our imaging parameters. Combining fringe removal and maximum-likelihood estimation, we have improved our signal-to-noise ratio by a factor of 3, allowing for atom-shot-noise-limited detection of ensembles comprising as few as 270 atoms, a factor of 9 lower than without these methods. Averaging measurements from both mirror images would offer a further $\sqrt{2}$ improvement in SNR.

The sensitivity could be improved to the single-atom regime by increasing the imaging resolution and better localizing the atoms. Optimal imaging parameters are found by considering a model for blurring due to photon recoil after release from the trap, where the cloud size a increases proportionally to $s\tau^3/(1+s)$. Integrated photon shot noise scales with $\sqrt{a(1+s)^2/s\tau}$, yielding an optimal saturation parameter of $s_{\mathrm{opt}} = 2/3$. For realistic imaging parameters (optical resolution of 1.2 μm, quantum efficiency of 0.9, and $\alpha = 1$) we find an optimal exposure time of 13 μs and a single cloud detection limit of 0.5 atoms/shot.

The atom clouds we prepare are considerably elongated, highlighting the potential application of our analysis to the study of one-dimensional quantum gases. Applying maximum-likelihood estimation column by column, for our experimental conditions we infer a sensitivity of 0.8 atoms/μm. This is below the typical linear density required to reach the crossover from the weakly interacting to the strongly interacting regime on an atom chip [19], which could be directly imaged in a single realization.

We would like to thank N. J. van Druten for loan of the CCD camera and fruitful discussions. We are grateful to FOM and NWO for financial support. S.W. acknowledges support from the EU Marie-Curie program.

[1] I. Bloch, J. Dalibard, and W. Zwerger, Rev. Mod. Phys. **80**, 885 (2008).

[2] Y. Wang *et al.*, Phys. Rev. Lett. **94**, 090405 (2005); T. Schumm *et al.*, Nature Phys. **1**, 57 (2005); G. Jo *et al.*, Phys. Rev. Lett. **98**, 030407 (2007).

[3] D. M. Harber, H. J. Lewandowski, J. M. McGuirk, and E. A. Cornell, Phys. Rev. A **66**, 053616 (2002); P. Treutlein, P. Hommelhoff, T. Steinmetz, T. W. Hansch, and J. Reichel, Phys. Rev. Lett. **92**, 203005 (2004); R. P. Anderson, C. Ticknor, A. I. Sidorov, and B. V. Hall, Phys. Rev. A **80**, 023603 (2009); C. Deutsch *et al.*, Phys. Rev. Lett. **105**, 020401 (2010).

[4] J. Estève *et al.*, Nature (London) **455**, 1216 (2008); J. Appel *et al.*, Proc. Natl. Acad. Sci. USA **106**, 10960 (2009); M. F. Riedel *et al.*, Nature (London) **464**, 1170 (2010); C. Gross *et al.*, *ibid.* **464**, 1165 (2010); I. D. Leroux, M. H. Schleier-Smith, and V. Vuletić, Phys. Rev. Lett. **104**, 073602 (2010).

[5] M. Albiez *et al.*, Phys. Rev. Lett. **95**, 010402 (2005).

[6] B. V. Hall, S. Whitlock, R. Anderson, P. Hannaford, and A. I. Sidorov, Phys. Rev. Lett. **98**, 030402 (2007).

[7] S. Levy *et al.*, Nature (London) **449**, 579 (2007).

[8] S. M. Kay, *Fundamentals of Statistical Signal Processing: Estimation Theory* (Prentice-Hall, Upper Saddle River, NJ, 1993).

[9] R. Gerritsma *et al.*, Phys. Rev. A **76**, 033408 (2007); S. Whitlock *et al.*, New J. Phys. **11**, 023021 (2009).

[10] S. Whitlock, C. F. Ockeloen, and R. J. C. Spreeuw, Phys. Rev. Lett. **104**, 120402 (2010).

[11] G. Reinaudi *et al.*, Opt. Lett. **32**, 3143 (2007).

[12] S. Schneider *et al.*, Phys. Rev. A **67**, 023612 (2003).

[13] The idea of the algorithm originates from M. Erhard, Ph.D. thesis, Universität Hamburg, 2004; J. Kronjäger, Ph.D. thesis, Universität Hamburg, 2007.

[14] X.-L. Li, M. Ke, B. Yan, and Y.-Z. Wang, Chin. Opt. Lett. **5**, 128 (2007).

[15] L. Sirovich and M. Kirby, J. Opt. Soc. Am. A **4**, 519 (1987).

[16] D. Lafrenière *et al.*, Astrophys. J. **660**, 770 (2007).

[17] G. H. Golub and C. F. Van Loan, *Matrix Computations*, 3rd ed. (Johns Hopkins University Press, Baltimore, MD, 1996).

[18] S. R. Segal, Q. Diot, E. A. Cornell, A. A. Zozulya, and D. Z. Anderson, Phys. Rev. A **81**, 053601 (2010).

[19] M. Olshanii, Phys. Rev. Lett. **81**, 938 (1998); J. Reichel and J. Thywissen, J. Phys. IV (France) **116**, 265 (2004); J. J. P. van Es *et al.*, J. Phys. B **43**, 155002 (2010).